ISSN 1063-7788, Physics of Atomic Nuclei, 2014, Vol. 77, No. 11, pp. 1313–1320. © Pleiades Publishing, Ltd., 2014.
Original Russian Text © A.S. Danagulyan, G.H. Hovhannisyan, T.M. Bakhshiyan, R.H. Avagyan, A.E. Avetisyan, I.A. Kerobyan, R.K. Dallakyan, 2014, published in Yadernaya Fizika, 2014, Vol. 77, No. 11, pp. 1378–1385.

NUCLEI
Experiment

Photonuclear Reactions on ^{112,118,124}Sn, ^{nat}Te, and ^{nat}Hf Targets

A. S. Danagulyan[1)], G. H. Hovhannisyan[1)*], T. M. Bakhshiyan[1)], R. H. Avagyan[2)], A. E. Avetisyan[2)], I. A. Kerobyan[2)], and R. K. Dallakyan[2)]

Received December 20, 2013; in final form, March 11, 2014

Abstract—The yields of products of photonuclear reactions on tin targets enriched in the isotopes ^{112,118,124}Sn and on Te and HfO_2 targets of natural isotopic composition were measured. The targets were irradiated at the linear electron accelerator of the A.I. Alikhanian National Science Laboratory (Yerevan Physics Institute) at the electron energy of $E_e = 40$ MeV. The dependence of the product yields on the nucleonic composition of the targets was discussed. The isomeric ratios were obtained for the ^{119m,g}Te, ^{121m,g}Te, ^{117m,g}In, and ^{123m,g}Sn products. The experimental data in question were compared with their theoretical counterparts calculated on the basis of the TALYS 1.4 code. The dependence of the isomeric ratios on the photon energy and on the mass number of the product is considered.

DOI: 10.1134/S1063778814100056

INTRODUCTION

Photonuclear reactions at intermediate energies have vigorously been studied for many years. Owing to those studies, it became possible to determine some general properties of nuclei and parameters of their individual levels. This served as a good basis for developing and refining various theoretical models. At the present time, there exist publications and international databases that combine all available experimental data on photonuclear reactions at energies lying in the region of and higher than the giant-dipole-resonance energy [1, 2]. However, some reactions have not yet been studied. For example, there are no experimental data on the yields of ^{173,175}Hf products that would originate from (γ, n) and (γ, p) reactions [1, 2]. The objective of the present study was to measure the yields of products of reactions that proceed on ^{112,118,124}Sn, ^{nat}Te, and ^{nat}Hf targets for the case where the endpoint energy of the bremsstrahlung spectrum is $E_{\gamma\,\max} = 40$ MeV, as well as to measure and analyze the isomeric ratios for the products of the reactions ^{120}Te$(\gamma, n)^{119m,g}$Te, ^{122}Te$(\gamma, n)^{121m,g}$Te, ^{118}Sn$(\gamma, p)^{117m,g}$In, and ^{124}Sn$(\gamma, n)^{123m,g}$Sn and to compare the resulting experimental data with their counterparts calculated on the basis of the TALYS 1.4 code. Currently available data on the isomeric ratios for the reactions ^{120}Te$(\gamma, n)^{119m,g}$Te and ^{122}Te$(\gamma, n)^{121m,g}$Te are limited to giant resonance region [3–6], while data on the isomeric ratios for the reactions ^{118}Sn$(\gamma, p)^{117m,g}$In are very fragmentary [4, 5, 7–12]; finally, data on the isomeric ratios for the reactions ^{124}Sn$(\gamma, n)^{123m,g}$Sn are scanty [3, 10]. An investigation of isomeric ratios would provide information both about the reaction mechanism and about the energy levels of the excited nucleus involved.

DESCRIPTION OF THE EXPERIMENT

The targets under study were manufactured from tin enriched in the isotopes ^{112,118,124}Sn and from Te and HfO_2 of natural isotopic composition and were irradiated at the linear electron accelerator (LUE-50) of the A.I. Alikhanian National Science Laboratory (Yerevan Physics Institute) at the electron energy of $E_e = 40$ MeV, the average current being 10 μA. A description of the experimental setup used in our experiment can be found in [13]. The converter material and thickness were chosen on the basis of a simulation. The optimum thickness of the tantalum converter was calculated with the aid of the GEANT4 package. The result proved to be 2 mm.

The beam intensity N_γ was determined by means of a monitoring reaction. A foil of natural copper 50 μm thick was chosen as a monitor target. The ^{112,118,124}Sn targets were also fabricated in the form of thin foils. In order to prepare targets from HfO_2 and ^{nat}Te, a powder material was pressed into tablets. The properties of the targets (degree of enrichment, thickness, and weight) are listed in Table 1.

[1)]Yerevan State University, Alex Manoogian str. 1, Yerevan 0025, Republic of Armenia.
[2)]A.I. Alikhanian National Science Laboratory (Yerevan Physics Institute) (YerPhi), Alikhanian Brothers str. 2, Yerevan 0036, Republic of Armenia.
[*]E-mail: hov_gohar@ysu.am

Table 1. Degree of enrichment or isotopic composition of targets, their weight, and their thickness

Target	Enrichment or composition, %	Target thickness, μm	Target weight, g
^{112}Sn	91	100	0.163
^{118}Sn	98.5	100	0.167
^{124}Sn	91.9	100	0.161
^{nat}Te	^{120}Te—0.096 ^{122}Te—2.603 ^{123}Te—0.908 ^{124}Te—4.816 ^{125}Te—7.139 ^{126}Te—18.95 ^{128}Te—31.69 ^{130}Te—33.80	300	1.48
HfO_2	^{174}Hf—0.162 ^{176}Hf—5.206 ^{177}Hf—18.606 ^{178}Hf—27.297 ^{179}Hf—13.629 ^{180}Hf—35.100	300	1.36

Two irradiation runs were performed. In the first run, the monitoring target and the HfO_2, Te, and ^{112}Sn targets were irradiated for 18 minutes. The copper target was at a frontal position. In the second run, the monitoring target and the HfO_2, Te, and ^{118,124}Sn targets were irradiated for 44 minutes. The number of photons incident to the monitoring target was assumed to be identical to the number of photons incident to the remaining targets, since all of the targets were thin, so that photon absorption was insignificant. The yields of the monitoring reactions were given in [14]. They are 53 mb for the reaction ^{65}Cu$(\gamma, n)^{64}$Cu and 2.6 mb for the reaction ^{63}Cu$(\gamma, 2n)^{61}$Cu. The beam intensity was estimated at 1.06×10^{16} and 2.35×10^{15} photons per hour for, respectively, the first and the second irradiation run.

The activity induced in the targets was measured with the aid of a high-purity germanium (HpGe) detector. The efficiency of photon detection was determined by using reference spectrometric gamma sources (RSGS). The detector efficiency was 1.66 keV for the 1.33-MeV line and 618-eV for the 122 keV line.

The reaction yield was calculated by the formula

$$Y = \Delta N\lambda/(N_\gamma N_{\rm nucl} k\varepsilon\eta(1 - e^{-\lambda t_1}) \times e^{-\lambda t_2}(1 - e^{-\lambda t_3})), \quad (1)$$

where ΔN is the total number of events under the photopeak according to measurements with a detector over the time t_3; λ is the decay constant; N_γ is the number of photons in the beam per hour; $N_{\rm nucl}$ is the number of target nuclei per 1 cm^2; k is the coefficient of photon absorption in the target, in air, and in the detector lid; ε is the photon-detection efficiency; η is the partial intensity of the product gamma line; t_1 is the irradiation time; t_2 is the time interval between the completion of an irradiation run and the beginning of measurements; and t_3 is the measurement time.

DISCUSSION OF THE RESULTS

The yields of photonuclear reactions proceeding on tin targets enriched in the isotopes ^{112,118,124}Sn and on Te and HfO_2 targets of natural isotopic composition are presented in Table 2. For the products in question, this table gives the half-lives, characteristic gamma lines, and their intensities, as well as the reactions that lead to the formation of these products. It should be noted that the yield of the reaction ^{112}Sn$(\gamma, n)^{111}$Sn cannot be measured since the ^{111}Sn nucleus do not feature a gamma line convenient for detection and has a half-life of $T_{1/2} = 35$ min, undergoing a transition to a ^{111}In nucleus. As a result, ^{111}In is formed as the product of the reaction ^{112}Sn$(\gamma, p)^{111}$In and as the product of decay of a ^{111}Sn parent nucleus and is detected experimentally as the summed yield. One can estimate the yield of the reaction ^{112}Sn$(\gamma, n)^{111}$Sn, considering that, at $E_{\gamma\,\max} = 40$ MeV, the yield of the (γ, n) reaction on a ^{112}Sn nucleus is approximately one order of magnitude greater than the yield of the respective (γ, p) reaction [2].

Analyzing our results, we can notice that, basically, the (γ, n) yields grow with the target mass number A_t. The reason is that, as the mass number grows, the respective nuclei become neutron-rich. Figure 1 shows the dependence of the (γ, n) yields on the product mass number $(A_t - 1)$. In addition to our results, this figure also gives data from [14]. The (γ, n) yields grow linearly as the target mass number increases. The ^{47}Ca and ^{123}Sn products originating from the highly neutron-rich nuclei of, respectively, ^{48}Ca and ^{124}Sn [$N/Z(^{48}\text{Ca}) = 1.4$ and $N/Z(^{124}\text{Sn}) = 1.48$] do not fit in the general dependence. The yields of the ^{119}Te, ^{121}Te, ^{129}Te, ^{173}Hf, and ^{175}Hf products lie lower since these products come from targets of natural isotopic composition. However, an increase in the yield of these products as the target mass number (or the number of neutrons in the target nucleus) grows is obvious.

The (γ, p) yields are substantially lower than the (γ, n) yields and show a trend toward a decrease as the target mass number increases (see Table 2).

For some residual nuclei (^{119}Te, ^{121}Te, ^{117}In, and ^{123}Sn), we obtained the yields of the ground (Y_g) and

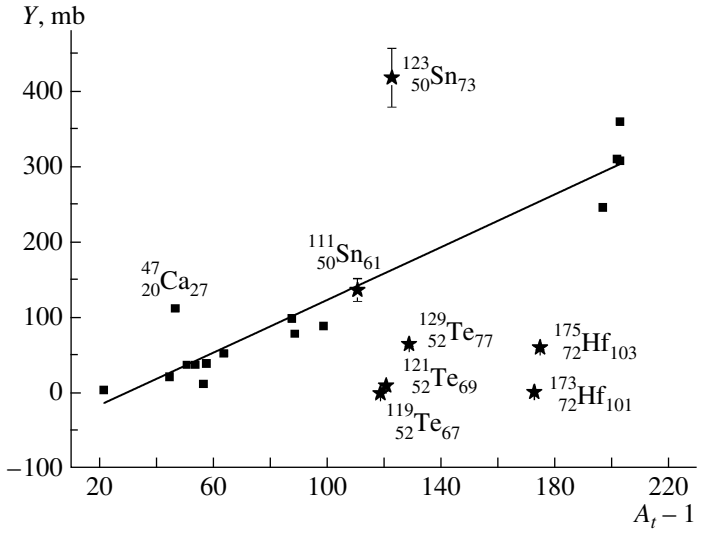

Fig. 1. Dependence of the (γ, n) yields on the product mass number $(A_t - 1)$.

isomeric (Y_m) states. The ratio of the yields of high- and low-spin states (Y_h/Y_l), which is also known as the isomeric ratio, depends, first of all, on the photonuclear-reaction mechanism. A comparison of experimental data with model predictions makes it possible to find out whether the choice of mechanism was correct. Investigation of the isomeric states of nuclei also provides information that makes it possible to refine the form of the level-density distribution for excited states of nuclei.

Table 3 gives values obtained for the isomeric ratios in question. The products being considered are formed in reactions involving the emission of one or several nucleons and are characterized by isomeric-ratio values less than unity (see Table 3); that is, high-spin states are populated with a lower probability.

We can interpret our results on the basis of the statistical model of a compound nucleus. As the result of an intranuclear cascade, high-energy nucleons escape from the target nucleus, leaving it with a high excitation energy and angular momentum. The subsequent evaporation stage involves the emission of low-energy nucleons and photons. As the number of emitted particles increases, the initial spin distribution becomes broader. It follows that, as the number of cascade particles increases, the high-spin state arises with a higher probability in relation to the low-spin state. Thus, the isomeric ratios for products of the cascade–evaporation process have values greater than unity. If products originate from simple reactions involving the emission of a small number of nucleons, it would be natural to expect isomeric-ratio values below unity [15, 16].

In order to compare the experimental data that we obtained with theoretical results, we have performed calculations with the aid of the TALYS 1.4 code. In order to calculate cross sections and yields on the basis of the statistical model, one needs information about the energy levels of the excited after-cascade nucleus. If information about discrete excited levels is unavailable or incomplete, then one performs calculations with some distribution of the level density in the form of an analytic dependence of the level density on the excitation energy, spin, and parity of levels.

In relation to TALYS 1.2, the TALYS 1.4 code offers wider possibilities for the choice of form for the distribution of the level density [17]. TALYS 1.4 contains five different models for the distribution of the level density. Three of them are phenomenological models yielding somewhat different forms of the distribution. These are the constant temperature + Fermi gas model [in Table 3 and in Fig. 2, this is model (1)], the back-shifted Fermi gas model [model (2)], and the generalized superfluid model [model (3)]. The distribution of the level density involves a spin cutoff parameter that determines the width of the angular-momentum distribution. In the microscopic calculations, it was noticed that the spin cutoff parameter depends on shell effects. The TALYS 1.4 code makes it possible to perform calculations by using both a spin cutoff parameter that depends on shell effects (spin-cut model 1) and a spin cutoff parameter that does not depend on them (spin-cut model 2) [17]. In Table 3, these are models (6) and (7), respectively.

The other two models for the distribution of the level density rely on microscopic approaches. One of them employs the microscopic level densities from Goriely's table [model (4) in Table 3], which contains level densities obtained for excitation energies of up to 150 MeV and spin values of up $J = 30$ on the basis

Table 2. Yields of photonuclear reactions on targets from tin enriched in the isotopes ^{112,118,124}Sn and from Te and HfO_2 of natural isotopic composition

Nuclear product	$T_{1/2}$	Spin and parity	E_γ, keV	I, %	Reaction type	Yield σ, mb
^{110}Sn	4.11 h	0^+	280.462	100	$^{112}\mathrm{Sn}(\gamma,2n)^{110}\mathrm{Sn}$	3.2 ± 0.3
^{117m}In	116.2 min	$1/2^-$	158.56 315.302	16 19.1	$^{118}\mathrm{Sn}(\gamma,p)^{117m}\mathrm{In}$	1.4 ± 0.14
^{117g}In	43.2 min	$9/2^+$	158.56 552.9	87 100	$^{118}\mathrm{Sn}(\gamma,p)^{117g}\mathrm{In}$	1.25 ± 0.12
^{123m}Sn	40.06 min	$3/2^+$	160.33	86	$^{124}\mathrm{Sn}(\gamma,n)^{123m}\mathrm{Sn}$	280 ± 25
^{123g}Sn	129.2 d	$11/2^-$	1088.64	0.6	$^{124}\mathrm{Sn}(\gamma,n)^{123g}\mathrm{Sn}$	138 ± 40
^{123m}Te	119.7 d	$11/2^-$	158.97	84	$^{124}\mathrm{Te}(\gamma,n)^{123m}\mathrm{Te}$ $^{125}\mathrm{Te}(\gamma,2n)^{123m}\mathrm{Te}$ $^{126}\mathrm{Te}(\gamma,3n)^{123m}\mathrm{Te}$	5.3 ± 0.6
^{121m}Te	154 d	$11/2^-$	212.189	81.4	$^{122}\mathrm{Te}(\gamma,n)^{121m}\mathrm{Te}$ $^{124}\mathrm{Te}(\gamma,3n)^{121m}\mathrm{Te}$	1.6 ± 0.2
^{121g}Te	16.78 d	$1/2^+$	507.591 573.139	17.7 80.3	$^{122}\mathrm{Te}(\gamma,n)^{121g}\mathrm{Te}$ $^{124}\mathrm{Te}(\gamma,3n)^{121g}\mathrm{Te}$	9.0 ± 0.8
^{119m}Te	4.7 d	$11/2^-$	270.53 1212.73	28 66	$^{120}\mathrm{Te}(\gamma,n)^{119m}\mathrm{Te}$ $^{122}\mathrm{Te}(\gamma,3n)^{119m}\mathrm{Te}$	0.075 ± 0.008
^{119g}Te	16.03 h	$1/2^+$	644.01	84	$^{120}\mathrm{Te}(\gamma,n)^{119g}\mathrm{Te}$ $^{122}\mathrm{Te}(\gamma,3n)^{119g}\mathrm{Te}$	0.75 ± 0.07
^{129m}Te	33.6 d	11/2-	459.6	4.93	$^{130}\mathrm{Te}(\gamma,n)^{129m}\mathrm{Te}$	23.3 ± 3
^{126g}Sb	12.46 d	8^-	666.3 414.81	100 83.3	$^{128}\mathrm{Te}(\gamma,pn)^{126g}\mathrm{Sb}$ $^{130}\mathrm{Te}(\gamma,p3n)^{126g}\mathrm{Sb}$	0.06 ± 0.008
^{127}Sb	3.85 d	$7/2^+$	473 685.7 783.7	25.7 37 15	$^{128}\mathrm{Te}(\gamma,p)^{127}\mathrm{Sb}$ $^{130}\mathrm{Te}(\gamma,p2n)^{127}\mathrm{Sb}$	1.2 ± 0.15
^{129g}Sb	4.4 h	$7/2^+$	812.8 544.7	43 17.9	$^{130}\mathrm{Te}(\gamma,p)^{129}\mathrm{Sb}$	0.27 ± 0.02
^{173}Hf	23.6 h	$1/2^-$	296.974	33.9	$^{174}\mathrm{Hf}(\gamma,n)^{173}\mathrm{Hf}$ $^{176}\mathrm{Hf}(\gamma,3n)^{173}\mathrm{Hf}$	2.1 ± 0.2
^{175}Hf	70 d	$5/2^-$	343.4	84	$^{176}\mathrm{Hf}(\gamma,n)^{175}\mathrm{Hf}$ $^{177}\mathrm{Hf}(\gamma,2n)^{175}\mathrm{Hf}$ $^{178}\mathrm{Hf}(\gamma,3n)^{175}\mathrm{Hf}$	61 ± 3
^{179}Lu	4.59 h	$7/2^+$	214.33	11.3	$^{180}\mathrm{Hf}(\gamma,p)^{179}\mathrm{Lu}$	4.0 ± 0.4

of Hartree–Fock calculations [17]. The other microscopic model, that of microscopic level densities from Hilaire's table [model (5) in Table 3], includes detailed calculations of intrinsic nuclear-level densities and of changes induced by collective effects. Level densities for more than 8500 nuclei are available in a tabulated form at excitation energies of up to 200 MeV and spin values of up to $J = 49$.

The TALYS 1.4 code makes it possible to calculate cross sections for ground and isomeric states of residual nuclei at specific energies. But in experiments based on the use of bremsstrahlung, one calculates

Table 3. Experimental values of the isomeric ratio (Y_h/Y_l) and their counterparts calculated on the basis of the TALYS 1.4 code

Nuclear product	Spin–parity of the ground and isomeric levels	ΔJ	Experiment	TALYS							
				(1)		(2)		(3)		(4)	(5)
				(6)	(7)	(6)	(7)	(6)	(7)		
^{117}In	$9/2^+$ $1/2^-$	4	0.89 ± 0.09	0.87	0.88	0.91	0.88	0.89	0.85	1.11	1.25
^{119}Te	$11/2^-$ $1/2^+$	5	0.10 ± 0.02	0.12	0.11	0.13	0.13	0.12	0.12	0.15	0.18
^{121}Te	$11/2^-$ $1/2^+$	5	0.18 ± 0.03	0.14	0.14	0.16	0.16	0.15	0.14	0.19	0.21
^{129}Te	$11/2^-$ $3/2^+$	4	0.55 ± 0.11*	0.08	0.09	0.1	0.1	0.09	0.1	0.16	0.13
^{123}Sn	$11/2^-$ $3/2^+$	4	0.49 ± 0.14	0.267	0.267	0.294	0.294	0.272	0.272	0.364	0.348

* Data on the yield of ^{129g}Te ($3/2^+$) were taken from [10].

the reaction yield, which is the convolution of the cross sections ($\sigma(E)$) with the photon spectrum (W) with respect to the energy (E); that is,

$$Y(E_{\gamma\,\max}) = a \int\limits_{E_{\rm thr}}^{E_{\gamma\,\max}} W(E_{\gamma\,\max}, E)\sigma(E)dE, \quad (2)$$

where $E_{\rm thr}$ is the reaction threshold, $E_{\gamma\,\max}$ is the endpoint energy of the bremsstrahlung spectrum, and a is a normalization factor.

Considering that $W(E_{\gamma\,\max}, E) \sim \text{const} \cdot (1/E_\gamma)$ in expression (2), calculating the cross sections σ_i for energies in the range from the reaction threshold to $E_{\gamma\,\max}$, and assuming that σ_i are constant within a narrow interval of width 1 MeV, we can go over from cross sections to yields; that is,

$$Y(E_{\gamma\,\max}) = a \int\limits_{E_{\rm th}}^{E_{\gamma\,\max}} W(E_{\gamma\,\max}, E)\sigma(E)dE \quad (3)$$
$$= b\sum_i \sigma_i \int\limits_{E_1}^{E_2} \frac{1}{E}dE,$$

where b is a constant, whose value is immaterial in calculating isomeric ratios.

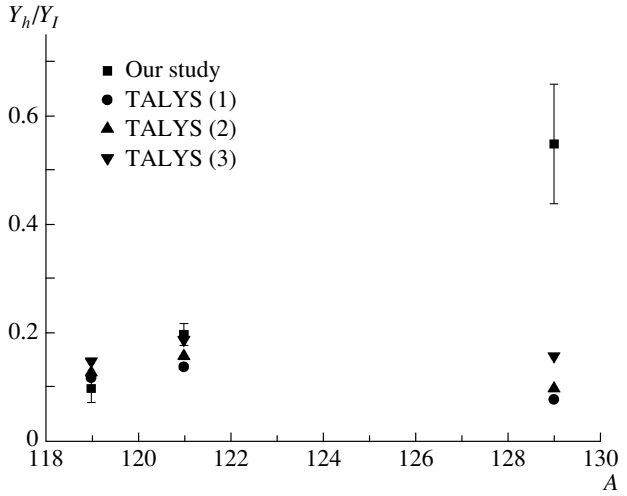

Fig. 2. Isomeric ratio as a function of the product mass number for tellurium isotopes.

Table 3 gives experimental values of the isomeric ratios (Y_h/Y_l) and their counterparts calculated in the way outlined above by using all possible models for the distribution of the level density. For phenomenological models, we performed calculations, choosing the aforementioned two forms for the spin cutoff parameter [17].

It should be noted that tellurium of natural isotopic composition was used as a target in the present study. In this case, the isotopes ^{119m,g}Te and ^{121m,g}Te may originate from the (γ, n) and $(\gamma, 3n)$ channels. Since the thresholds of the $(\gamma, 3n)$ reactions being considered are about 30 MeV and since the (γ, n) cross sections exceed substantially the $(\gamma, 3n)$ cross sections [2], we can assume, however, that the respective (γ, n) reactions are a dominant channel of ^{119m,g}Te and ^{121m,g}Te production.

One can see that the isomeric-ratio values obtained on the basis of the above phenomenological models differ only slightly from one another and, in

all cases, are smaller than the values obtained on the basis of microscopic models. The largest discrepancies between the experimental and calculated data are observed for the ^{129}Te and ^{123}Sn neutron-rich nuclei. For the ^{117}In nucleus, the microscopic models yield isomeric ratios in excess of unity, but this does not comply with experimental data. In the remaining cases, agreement is satisfactory.

Some authors discussed the dependence of the isomeric ratios on the spin difference ΔJ between the isomeric and ground states. A decrease in the isomeric ratio with increasing ΔJ was noticed in [18] in considering (γ, γ') reactions at energies in the giant-resonance region. In [19], a similar dependence was observed in the energy range of 100–500 MeV. According to our experimental results (see Table 3), smaller values of the isomeric ratio correspond to larger values of the spin difference.

If one considers the same reaction type at identical excitation energies and identical spins of the initial and final states, then the isomeric ratio depends on the structure of levels through which the isomeric state is populated [18]. Figure 2 gives the isomeric ratios for tellurium isotopes according to measurements in the respective (γ, n) reactions at $E_{\gamma\,\max} = 40$ MeV. In the isomeric state, the nuclei being considered have a spin of $11/2^-$; in the ground state, the ^{119}Te and ^{121}Te nuclei have a spin of $1/2^+$, while the ^{129}Te nucleus has a spin of $3/2^+$. One can see that, for tellurium nuclei, which lie in the vicinity of the tin nucleus closed in the number of protons and which have a moderately small value of the deformation parameter, the isomeric ratio grows with the number of neutrons. A similar dependence was also noticed in [18, 20] at $E_{\gamma\,\max} = 25$ MeV.

In addition to experimental data, Fig. 2 gives the isomeric-ratio values calculated on the basis of the TALYS 1.4 code by using the above three phenomenological models for the distribution of the level density. We can say that the results obtained on the basis of these models comply well with experimental data in the case of ^{119}Te and ^{121}Te nuclei, but, in the case of the ^{129}Te nucleus, the experimental values are nearly five times as great as their model-based counterparts. We note that the experimental values presented for the isomeric ratio in [4, 10] for ^{129}Te at the energies of $E_{\gamma\,\max} = 30$ and 50 MeV agree with those in Fig. 2 within 10 to 12%.

The experimental data that we obtained reveal that, for tellurium nuclei, the isomeric ratios grow as the number of neutrons increases. The model predictions do not reflect this dependence. Since the isomeric ratio depends on the structure of low-lying levels from which the last transition to the ground or isomeric state proceeds, we can assume that the discrepancy in question may stem from an inaccurate model description of the level densities as the filling of neutron shells occurs.

Let us now consider the dependence of the isomeric ratios of the product yields on the endpoint energy of the bremsstrahlung spectrum. According to [18, 20], the isomeric ratios for (γ, n) reactions grow with energy in the region of the giant dipole resonance. Figure 3 shows the isomeric ratio as a function of the endpoint energy of the bremsstrahlung spectrum for the reactions $^{120}\mathrm{Te}(\gamma, n)^{119m,g}\mathrm{Te}$ and $^{122}\mathrm{Te}(\gamma, n)^{121m,g}\mathrm{Te}$. In addition to the results that we obtained, we used data from [3–6]. Available experimental data are basically well-consistent, with the exception of data from [4], where the authors presented isomeric-ratio values in excess of unity for the reaction $^{120}\mathrm{Te}(\gamma, n)^{119m,g}\mathrm{Te}$. One observes a steep growth of the isomeric ratios between the threshold and the giant-dipole-resonance energy, whereupon the growth becomes slower; at $E_{\gamma\,\max} = 40$ MeV, the isomeric ratio decreases somewhat. The ascending character of the curves is obviously due to an increase in the excitation energy of the residual nucleus in which a photon cascade develops. As the endpoint energy of the bremsstrahlung spectrum increases (starting from an energy of 25 MeV), the contribution of direct neutron-emission processes increases, especially for near-magic nuclei, leading to a decrease in the probability for the formation of a high-spin nuclear state [18]. Data available in the literature on the isomeric ratios for the reactions $^{130}\mathrm{Te}(\gamma, n)^{129m,g}\mathrm{Te}$ in the energy range that extends to $E_{\gamma\,\max} = 72$ MeV and where one clearly sees a similar dependence were compiled in [21].

Figure 3 also shows data obtained with the aid of the TALYS 1.4 code. In the region of energies above the energy corresponding to the dipole-resonance maximum, the theoretical curves lie lower that their experimental counterparts. Starting from an energy of about 25 MeV, the calculated isomeric ratios undergo virtually no change, whereas the respective experimental values decrease somewhat.

For the ^{117m,g}In isomeric pair, the spin of the isomeric state ($1/2^-$) is smaller than the ground-state spin ($9/2^+$). Values of the ratios Y_m/Y_g are given in some articles [4, 5, 8, 9, 12], while the ratios of the yields of high- and low-spin states (Y_h/Y_l) are considered in [10, 11] and in the present study. Upon rescaling available data on the isomeric ratios for the reactions $^{118}\mathrm{Sn}(\gamma, p)^{117m,g}\mathrm{In}$ to the form Y_h/Y_l, one can trace a dependence similar to the dependence in the preceding figures, even though the scatter of the data is quite significant (Fig. 4). At high energies, the growth of the isomeric ratio as a function of $E_{\gamma\,\max}$ is

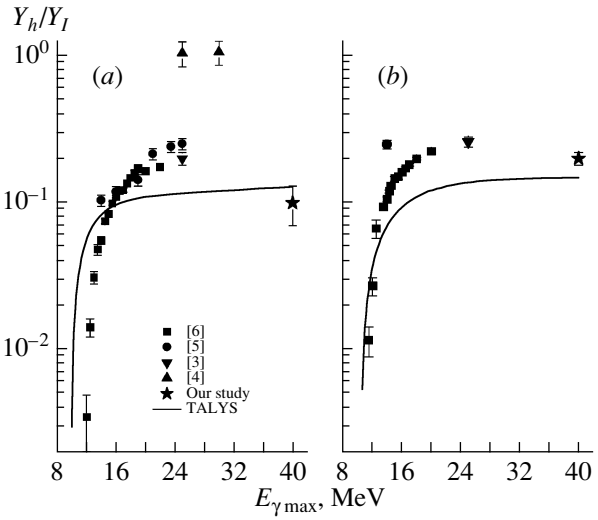

Fig. 3. Isomeric ratio as a function of the endpoint energy of the bremsstrahlung spectrum for the reactions (*a*) ^{120}Te$(\gamma, n)^{119m,g}$Te and (*b*) ^{122}Te$(\gamma, n)^{121m,g}$Te.

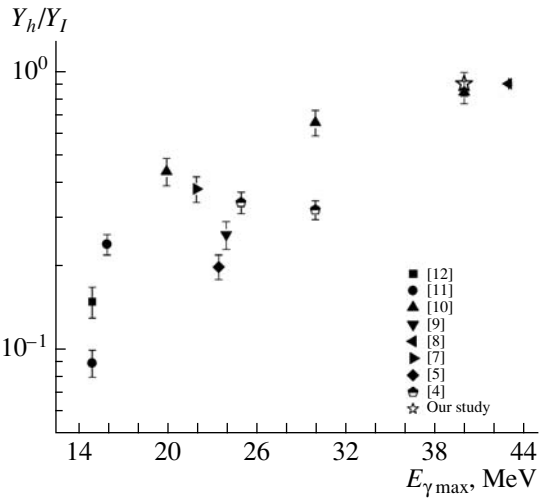

Fig. 4. As in Fig. 3, but for the reaction ^{118}Sn$(\gamma, p)^{117m,g}$In.

expected to become slower because of the contribution of direct proton-emission processes. This is due to the existence of the Coulomb barrier.

CONCLUSIONS

Our analysis of data on the yields of photonuclear reactions, including reactions that lead to the excitation of isomeric states, and a comparison with data obtained by using the TALYS 1.4 code have led to the following conclusions:

(i) The yields of (γ, n) reactions grow as the number of neutrons in the target nucleus increases. The yields of (γ, p) reactions show a trend toward a decrease with increasing number of neutrons in the target nucleus.

(ii) For tellurium nuclei, which lie in the vicinity of the tin nucleus closed in the number of protons and which have a moderately small deformation parameter, the isomeric ratio grows as the number of neutrons increases. The data calculated by using the TALYS 1.4 code do not exhibit such a dependence. This discrepancy may be due to the use of an inaccurate model description of the level density.

(iii) The isomeric ratios for the (γ, n) products grow with increasing endpoint energy of the bremsstrahlung spectrum, this growth persisting up to the upper boundary of the giant-dipole-resonance region. As the energy grows further, the isomeric ratios exhibit a modest decrease associated with the increase in the contribution of direct processes, but this does not occur in the data calculated with the aid of the TALYS 1.4 code.

ACKNOWLEDGMENTS

We are grateful to the headquarters and whole staff of the Accelerator Department of the Alikhanian National Science Laboratory for ensuring good beam parameters.

REFERENCES

1. A. V. Varlamov, V. V. Varlamov, D. S. Rudenko, and M. E. Stepanov, *Atlas of Giant Dipole Resonances*, IAEA Nuclear Data Section (IAEA, 1999).
2. IAEA-TECHDOC-1178 (2000); http://www-pub.iaea.org/MTCD/Publications/PDF/te_1178_prn.pdf; https://www-nds.iaea.org/exfor/exfor.htm; http://cdfe.sinp.msu.ru/exfor/index.php
3. A. G. Belov, Yu. P. Gangrsky, A. P. Tonchev, and N. P. Balabanov, Phys. At. Nucl. **59**, 553 (1996).
4. S. R. Palvanov and O. Radzhabov, At. Energy **87**, 533 (1999).
5. Tran Duc Thiep, Truong Thi An, Nguyen Tuan Khai, et al., Phys. Part. Nucl. Lett. **6**, 126 (2009).
6. V. M. Mazur, Z. M. Bigan, D. M. Symochko, and T. V. Poltorzhits'ka, Phys. Part. Nucl. Lett. **9**, 248 (2012).
7. I. Z. Beseda, E. M. Bigan, V. S. Bokhinyuk, et al., in *Proceedings of the International Conference on Nuclear Spectroscopy and Nuclear Structure* (Nauka, St.-Petersburg, 1992), p. 245.
8. D. Kolev, E. Dobreva, N. Nenov, and V. Todorov, Nucl. Instrum. Methods Phys. Res. A **356**, 390 (1995).
9. Yu. P. Gangrsky, P. Zuzaan, N. N. Kolesnikov, et al., Phys. At. Nucl. **62**, 1615 (1999).
10. A. S. Danagulyan and N. A. Demekhina, Phys. At. Nucl. **60**, 1937 (1997); N. A. Demekhina, A. S. Danagulyan, and G. S. Karapetyan, Phys. At. Nucl. **65**, 365 (2002).

11. O. A. Bessheiko, I. N. Vishnevskii, V. A. Zheltonozhskii, et al., Bull. Russ. Acad. Sci.: Phys. **69**, 745 (2005).
12. I. N. Vishnevskii, V. A. Zheltonozhskii, I. N. Kadenko, et al., Bull. Russ. Acad. Sci.: Phys. **72**, 1569 (2008).
13. P. O. Avakyan, A. E. Avetisyan, I. A. Kerobyan, et al., J. Contemp. Phys. **47**, 5 (2012).
14. K. Masumoto, T. Kato, and N. Suzuki, Nucl. Instrum. Methods Phys. Res. **157**, 567 (1978).
15. R. Vandenbosch et al., Phys. Rev. **13**, 137 (1965).
16. A. S. Danagulyan and N. A. Demekhina, Sov. J. Nucl. Phys. **27**, 466 (1978); V. E. Aleksandryan, A. A. Arakelyan, and A. S. Danagulyan, Phys. At. Nucl. **56**, 707 (1993); A. S. Danagulyan, G. O. Oganesyan, A. R. Balabekyan, et al., Phys. At. Nucl. **76**, 349 (2013).
17. http://www.talys.eu/
18. Yu. P. Gangrsky, A. P. Tonchev, and N. P. Balabanov, Phys. Part. Nucl. **27**, 428 (1996).
19. B. L. Zhuikov and A. S. Iljinov, Phys. At. Nucl. **69**, 739 (2006).
20. V. M. Mazur, Phys. Part. Nucl. **31**, 188 (2000).
21. Tran Duc Thiep, Truong Thi An, Phan Viet Cuong, et al., J. Radioanal. Nucl. Chem. **289**, 637 (2011).